Çukurova Üniversitesi Mühendislik Mimarlık Fakültesi Dergisi, 33(4), ss. 67-82, Aralık 2018
Çukurova University Journal of the Faculty of Engineering and Architecture, 33(4), pp. 67-82, December 2018

Dynamic Modeling of Slider-Crank Mechanism for Selecting Input Parameters for Desired Piston Speeds: Lumped Mass Approach

Mehmet İlteriş SARIGEÇİLİ[*1], İbrahim Deniz AKÇALI[1]

[1]*Çukurova Üniversitesi, Mühendislik Fakültesi, Makine Mühendisliği Bölümü, Adana*

Geliş tarihi: 02.08.2018 Kabul tarihi: 25.12.2018

Abstract

Here the dynamic behavior of slider-crank mechanism with a driving force applied at crank-pin center, has been modeled to formulate the piston speed. In view of the abundance of the parameters involved, a lumped parameter approach has been preferred to obtain a compact equation in the form of a second order non-linear differential equation. The complexity of the resulting equation has mandated implementing a numerical solution technique by which the effects of the selected parameters on the piston speed have been investigated. Under similar conditions an experimental model has been prepared and the tests have been carried out to compare the results. Low error levels achieved in two results have demonstrated the validity of the developed model.

Keywords: Slider-crank mechanism, Dynamic model, Required piston speed, Lumped mass approach

İstenen Piston Hızları için Giriş Parametrelerinin Seçilmesi Amacıyla Krank-Biyel Mekanizmasının Dinamik Modellenmesi: Topaklanmış Kütle Yöntemi

Öz

Piston hızının çıkarılması için, krank-pim merkezine bir kuvvet uygulanan krank-biyel mekanizmasının dinamik davranışı modellenmiştir. Dahil edilen parametrelerin çokluğu göz önüne alındığında ikinci dereceden lineer olmayan bir diferansiyel denklem şeklinde kompakt bir denklem elde etmek için topaklanmış parametre yöntemi tercih edilmiştir. Elde edilen denklemin karmaşıklığı, bir sayısal çözüm yöntemi uygulamayı zorunlu kılmıştır. Bu yolla çalışmada seçilen parametrelerin piston hızı üzerindeki etkileri incelenmiştir. Benzer şartlar altında deneysel bir model hazırlanmış ve sonuçları karşılaştırmak için testler gerçekleştirilmiştir. İki sonuç arasında elde edilen düşük hata oranları geliştirilen modelin geçerliliğini kanıtlamıştır.

Anahtar Kelimeler: Krank-biyel mekanizması, Dinamik model, Piston hızı kontrolü, Topaklanmış kütle yaklaşımı

[*]Sorumlu yazar (Corresponding author): Mehmet İlteriş SARIGEÇİLİ, *msarigecili@cu.edu.tr*

1. INTRODUCTION

Slider-crank mechanisms which are used for either converting rotational motion into translational motion (as in internal combustion engines) or vice versa (as in pumps or compressors) are widely applied [1–2] in industry. Slider-crank mechanism is also used as a feeder [3] such that stock material is pushed towards processing machine. In the feeder application, the piston pushing force as well as the piston speed at different stages of the processing (i.e. raw stock material free motion, pushing the material against machine, etc.) is very critical for production quality. In a recent study [4], the process of obtaining constant pushing force in a feeder slider-crank mechanism has already been explained. However, studying piston speed requires development of dynamic model for feeder slider-crank mechanism. Once the model is obtained, design by analysis technique can be applied to determine the appropriate values of dimensional and operational parameters by evaluating their effects on piston speed within acceptable tolerance limits in the interval of operation.

In the literature, there are several studies concentrating on dynamic model of a slider-crank mechanism for realizing different objectives. Franco et al. [5] used a slider-crank mechanism as a hand-powered press used for producing straw bales. Halicioglu et al. [6] reported the design and analysis of a slider-crank mechanism actuated by a servo motor at crank and used as press for metal forming operations. Their study applied kinematics and dynamics of slider-crank mechanism available from the literature. Erkaya et al. [7] presented the dynamic analysis of both a conventional and a modified (with additional eccentric connector and planetary gears) slider-crank mechanism for internal combustion engines. Even though the inertial effects were taken into consideration the gravitational effects were neglected.

Ha et al. [8] developed the dynamic model of a slider-crank mechanism by taking into account mass, external force and motor electric input. The model was based on a crank driven by a servo motor with a piston sliding at zero eccentricity from the crank center as well as along the horizontal axis. For the development of the model, Hamilton's principle, Lagrange multiplier, geometric constraints and partitioning method were used. The obtained differential equation was solved by fourth order Runge-Kutta Method. Due to the complex nature of the non-linearity of the parameters, they applied real-coded genetic algorithm for identifying optimum parameters of the mechanism. On the other hand, Huang et al. [9] studied a spatial slider-crank mechanism for developing the dynamic model of it and similar procedures of the study of Ha et al. [8] were applied.

Fung et al. [10] reported on the dynamic model of an intermittent slider-crank mechanism driven by a permanent magnetic synchronous servo motor at crank with two different constraining stops for the slider. The connecting rod of the mechanism was made out of a pneumatic cylinder. Hence, as the slider was stopped the pneumatic cylinder was either contracted or extended by a pressure regulating valve, based on the motion characteristics. Fourth order Runge-Kutta Method was applied for the solution of the derived differential equations from Hamilton's principle. Silva et al. [11] developed a kinematic model of an inverted slider-crank mechanism where each link was represented as a vector and the corresponding kinematic parameters (i.e. position, velocity and acceleration) were found out by matrix operations. The obtained mathematical model has been solved by Runge-Kutta Method and the results were compared by multibody model developed in ADAMS/View. The comparison of the results showed that the errors were considerable.

Dynamic models used in the speed control of slider-crank mechanisms are also available. As an example, Yan and Chen [12] used Bezier curves in order to represent crank angular positions for attaining a desired piston speed trajectory. The input motion of the crank was provided by a servo motor controlled on the basis of a PID algorithm. Hence, the Bezier parameters as well as PID parameters had to be optimized for the corresponding desired speed trajectory in their work. Lin et al. [13] proposed a fuzzy functional neural network position controller for slider-crank mechanism driven by a permanent magnet

synchronous servo motor. The dynamic model of the mechanism derived from Hamilton's principle and the Lagrange multiplier were used. It should be noted that a rotating disk was used as a crank in the model. On the other hand, Wai et al. [14] developed a fuzzy neural network controller with adaptive learning rate for the same type of mechanism with the same permanent magnet synchronous servo motor driver.

There are many studies that consider dynamic model of slider-crank mechanisms for the purposes of piston or joint lubrication. For example, Zhao et al. [15] used Lagrange multipliers and constraint Jacobian matrix for developing the dynamic equations of the slider-crank system. Hence, this dynamic model was coupled with the lubrication model of piston skirt-liner system. By this way, slap noise and lubrication performances could be evaluated with respect to several criteria such as design parameters of piston, bore clearance, bulge position and curvature parameter of piston skirt profile, etc. Reis et al. [16] developed the dynamic model of lubricated joints that have clearance in between piston-pin revolute joint and in a slider-crank mechanism of an internal combustion engine. The developed model takes into account the hydrodynamic effects as well as clearance and friction effects.

Several studies in the literature are reported on applying the developed dynamic model on vibration effects. For instance, Wang and Chen [17] developed dynamic model of a slider-crank mechanism with a composite coupler in the form of an axially periodic array for studying the parametric resonance of the mechanism. The developed model is based on Fourier-series approach and Newtonian mechanics. Akbari et al. [18] developed dynamic model of a slider-crank mechanism with a flexible coupler by using Euler-Lagrange method as well as the mode summation technique. Even though they analyzed the dynamic behavior of the mechanism, they also proposed two control methods for elastodynamic vibration suppression of the flexible coupler, with actuation at crank ground joint by an electric motor.

None of these studies answer the problem of obtaining a constant piston speed or a constant displacement for unit time interval in feeder slider-crank mechanisms. Hence, in this study, dynamic model of a slider-crank mechanism is obtained first. The resulting second order non-linear differential equation is solved by numerical methods. Then, an experimental setup is developed to validate the theoretical model results. In the results section, the effect of only crank position at the start of motion and externally added mass (out of 13 parameters) on piston speed are evaluated for obtaining the desired piston speed within allowable tolerance.

2. METHOD

In this paper, a slider-crank mechanism used as a feeder (Figure 1) is considered. The driving force on the slider-crank is made up of:

I. The constant F_B force with constant magnitude and constant line of action

II: Externally added mass m_B at the crank-pin center (point B) in the direction of producing static ($m_B g$) and dynamic ($m_B a_B$) effects with acceleration a_B at point B.

Hence, the driving force produces a non-linear forward translational piston motion. The rotational spring assembled to the crank at O has the tendency to obtain constant pushing force on the piston by balancing interacting forces developed due to the vertical force. When the mechanism is released at a particular position the piston gains speed. Hence, the problem is either obtaining a constant piston displacement from free motion in between each processing stage or obtaining acceptable constant piston speed for non-resistive / non-contact processing in between definite piston positions.

The links of the slider-crank mechanism in Figure 1 are identified as: link 1 is ground; link 2 is crank; link 3 is connecting rod; and link 4 is piston. The dimensions of the mechanism of interest are crank and connecting rod lengths (L_2 and L_3, respectively) and eccentricity between the crank center and piston line of action (L_4). The centers of gravity of crank and connecting rod are away from points O and B by r_{G2} and r_{G3}, respectively. The masses of crank, connecting rod and piston are represented by m_2, m_3, and m_4, respectively. The variables are crank angle

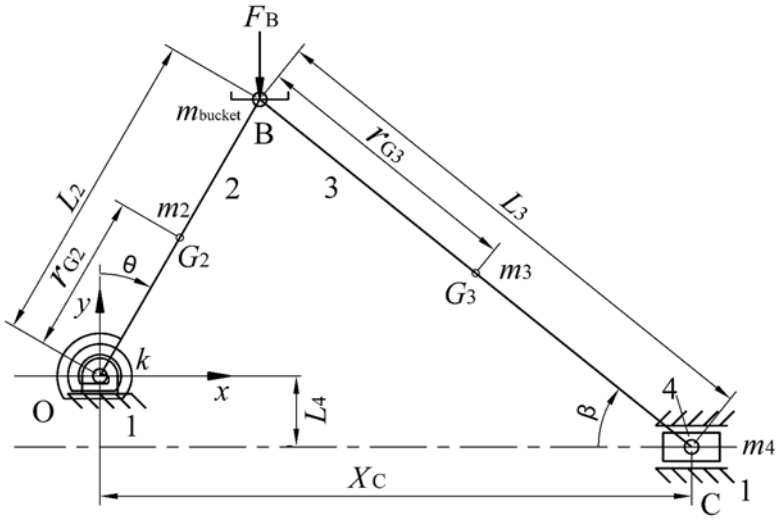

Figure 1. Slider-crank mechanism

θ and connecting rod angle β, with corresponding sign conventions. F_B represents external load applied whereas m_{bucket} stands for bare bucket mass.

In order to simplify the dynamic model of the slider-crank mechanism, the crank mass is lumped at points O and B while the connecting rod mass is lumped at points B and C. Hence, the total mass at point B makes only circular motion whereas the total mass at point C makes only translational motion.

The lumped mass of crank and connecting rod can be obtained by finding the statically equivalent mass systems [19]. The crank mass (m_2) can be replaced by a statically equivalent system lumped at points B (m_2^B) and O (m_2^O). The effect of crank mass at points B and O can be expressed as:

$$m_2^B = m_2 \frac{r_{G2}}{L_2} \tag{1}$$

$$m_2^O = m_2 - m_2^B \tag{2}$$

Similarly, the connecting rod mass (m_3) can be replaced by a statically equivalent system lumped at points B (m_3^B) and C (m_3^C). Hence, the effect of connecting rod mass at points B and C can be expressed by means of the following relationships:

$$m_3^B = m_3 \frac{L_3 - r_{G3}}{L_3} \tag{3}$$

$$m_3^C = m_3 - m_3^B \tag{4}$$

Resultantly, the masses can be considered as lumped at points A and B in the system as follows:

$$m_B = m_2^B + m_3^B + M_B \tag{5}$$

$$m_c = m_3^C + m_4 \tag{6}$$

whereas the lumped mass at point O (m_O) is defined by Eq. (2). It should be noted that M_B represents any external mass applied at point B including m_{bucket} to create a vertical downward force.

The next step would be to develop free body diagram (FBD) of each link (Figure 2) and analyze the equilibrium conditions. From FBD of link 4, the following two equations are obtained since there is no moment effect:

$$\underset{+}{\rightarrow}\sum F_x = 0 \quad F_{34x}\text{-}\mu F_{14}\text{-}m_C\ddot{X}_C=0 \tag{7}$$

$$+\uparrow \sum y = 0 \quad F_{34y} + F_{14} - m_C g = 0 \tag{8}$$

In a similar fashion, the equilibrium and D'Alembert equations are written for the connecting rod and crank by considering FBD of link 3 and link 2, respectively:

$$\rightarrow_{+}\sum F_x = 0 \qquad F_{43x} + F_{23x} = 0 \tag{9}$$

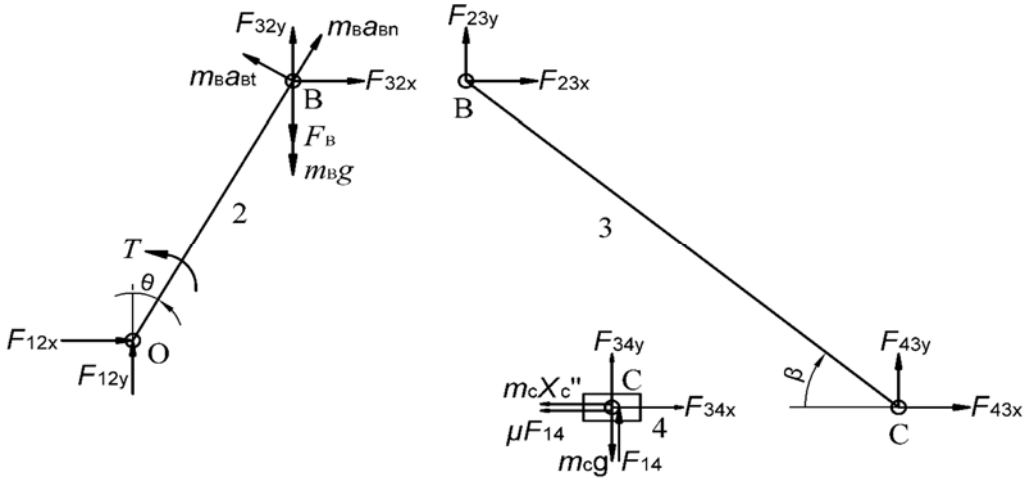

Figure 2. Free body diagram of each link in the slider – crank mechanism

$$+\uparrow\sum y = 0 \ldots F_{43_y} + F_{23_y} = 0 \tag{10}$$

$$\sum M_C = 0 \ldots F_{43_y} L_2 \cos\beta + F_{43x} L_2 \sin\beta = 0 \tag{11}$$

$$\rightarrow_{+}\sum F_x = 0 \quad \ldots \quad F_{32x}+F_{12x}-$$
$$m_B L_2 \ddot{\theta}\cos\theta + m_B L_2 \dot{\theta}^2 \sin\theta = 0 \tag{12}$$

$$+\uparrow\sum y = 0 \ldots F_{32y}+F_{12y}-F_B-$$
$$m_B g + m_B L_2 \ddot{\theta}\sin\theta + m_B L_2 \dot{\theta}^2 \cos\theta = 0 \tag{13}$$

$$\sum M_O = 0 \ldots T+m_B L_2{}^2\ddot{\theta}-F_{32x}L_2\cos\theta+F_{32y}L_2\sin\theta-$$
$$m_B g L_2 \sin\theta - F_B L_2 \sin\theta = 0 \tag{14}$$

It should be noted that normal and tangential accelerations at point B used in Eq. (14) are defined as:

$$a_{Bt} = L_2\alpha = L_2\ddot{\theta} \tag{15}$$

$$a_{Bn} = L_2\omega^2 = L_2\dot{\theta}^2 \tag{16}$$

Eqs. (7) and (8) can be rearranged to obtain:

$$F_{34x} = \mu F_{14} + m_C \ddot{X}_C \tag{17}$$

$$F_{34y} = m_C g - F_{14} \tag{18}$$

Recalling that the interacting joint forces should be equal and opposite to each other, Eqs. (17) and (18) can be substituted into Eq. (11) to obtain the following relation:

$$F_{34y} = -F_{34x}\tan\beta \tag{19}$$

Eqs. (17) – (19) can be solved for F_{14} as:

$$F_{14} = \frac{m_C g + m_C \ddot{X}_C \tan\beta}{1-\mu\tan\beta} \tag{20}$$

Substituting Eq. (20) into Eqs. (17) and (18) would yield:

$$F_{23x} = F_{34x} = m_C \ddot{X}_C + \mu\left(\frac{m_C g + m_C \ddot{X}_C \tan\beta}{1-\mu\tan\beta}\right) \tag{21}$$

$$F_{23y} = F_{34y} = m_C g - \frac{m_C g + m_C \ddot{X}_C \tan\beta}{1-\mu\tan\beta} \tag{22}$$

If the torque from spring acting on the crank is defined as in Eq. (23) and is substituted into Eq. (14), it will lead to Eq. (24):

$$T_2 = k\left(\theta - \theta_0^*\right) \tag{23}$$

$$k\left(\theta\text{-}\theta_0^*\right)+m_B{L_2}^2\ddot{\theta}+\left[m_C\ddot{X}_C+\mu\left(\frac{m_Cg+m_C\ddot{X}_C\tan\beta}{1-\mu\tan\beta}\right)\right]$$
$$L_2\cos\theta-\left[m_Cg-\frac{m_Cg+m_C\ddot{X}_C\tan\beta}{1-\mu\tan\beta}\right]L_2\sin\theta-$$
$$m_BgL_2\sin\theta-F_BL_2\sin\theta=0 \tag{24}$$

In Eqs. (23) & (24), k, θ and θ_0^* represent spring coefficient, crank angle and crank neutral angle for spring, respectively. The position of the piston (X_C) is given by Eq. (25). Piston speed ($\dot{X}_C$) and acceleration ($\ddot{X}_C$) can be found by taking first and second order derivative, respectively:

$$X_C = L_2\sin\theta + L_3\cos\beta \tag{25}$$

$$\dot{X}_C = L_2\cos\theta\,\dot{\theta} - L_3\sin\beta\,\dot{\beta} \tag{26}$$

$$\ddot{X}_C = -L_2\sin\theta\,\dot{\theta}^2 + L_2\cos\theta\,\ddot{\theta} - L_3\cos\beta\,\dot{\beta}^2 - L_3\sin\beta\,\ddot{\beta} \tag{27}$$

The relation in between the crank and connecting rod angular positions can be defined from Figure 1 as in Eq. (28) and it can be solved for β as in Eq. (29):

$$L_3\sin\beta = L_2\cos\theta + L_4 \tag{28}$$

$$\beta = \sin^{-1}\left[\frac{L_2\cos\theta + L_4}{L_3}\right] \tag{29}$$

By taking the first and second order derivatives of Eq. (28) and manipulating the obtained results would yield the connecting rod angular speed and accelerations as follows:

$$\dot{\beta} = -\frac{L_2}{L_3}\sin\theta\sec\beta\,\dot{\theta} \tag{30}$$

$$\ddot{\beta}=-\frac{L_2}{L_3}\cos\theta\sec\beta\,\dot{\theta}^2-$$
$$\frac{L_2}{L_3}\sin\theta\sec\beta\,\ddot{\theta}+\frac{{L_2}^2}{{L_3}^2}\sin^2\theta\sin\beta\sec^3\beta\,\dot{\theta}^2 \tag{31}$$

Substituting Eqs. (30) & (31) into Eq. (27) and further manipulation results in:

$$\ddot{X}_C=\dot{\theta}^2\left(-L_2\sin\theta-\frac{L_2^2}{L_3}\sin^2\theta\sec\beta+L_2\cos\theta\sin\beta\sec\beta-\right.$$
$$\left.\frac{{L_2}^2}{L_3}\sin^2\theta\sin^2\beta\sec^3\beta\right)+\ddot{\theta}(L_2\cos\theta+L_2\sin\theta\sin\beta\sec\beta) \tag{32}$$

Substituting Eq. (32) into Eq. (24) and further manipulation yields:

$$\left\{(1-\mu\tan\beta)\left[k\left(\theta\text{-}\theta_0^*\right)-m_BgL_2\sin\theta-F_BL_2\sin\theta\right]+\right.$$
$$\mu m_CgL_2\cos\theta+\mu m_CgL_2\sin\theta\tan\beta+\dot{\theta}^2\left(-\right.$$
$$m_C{L_2}^2\cos\theta\sin\theta-$$
$$m_C\frac{L_2^3}{L_3}\cos\theta\sin^2\theta\sec\beta+m_C{L_2}^2\cos^2\theta\tan\beta-$$
$$m_C\frac{{L_2}^3}{L_3}\cos\theta\sin^2\theta\tan^2\beta\sec\beta-m_C{L_2}^2\sin^2\theta\tan\beta-$$
$$m_C\frac{L_2^3}{L_3}\sin^3\theta\tan\beta\sec\beta+m_C{L_2}^2\sin\theta\cos\theta\tan^2\beta-$$
$$\left.m_C\frac{{L_2}^3}{L_3}\sin^3\theta\tan^3\beta\sec\beta\right)+$$
$$\left.\ddot{\theta}\begin{pmatrix}m_B{L_2}^2-\mu m_B{L_2}^2\tan\beta\\+m_C{L_2}^2\cos^2\theta\\+2m_C{L_2}^2\cos\theta\sin\theta\tan\beta\\+m_C{L_2}^2\sin^2\theta\tan^2\beta\end{pmatrix}\right\}/(1-$$
$$\mu\tan\beta) \tag{33}$$

where $(1-\mu\tan\beta)\neq 0$. Eq. (33) can be written as a second order non-linear differential equation as:

$$A_0(\theta)+A_1(\theta)\dot{\theta}^2+A_2(\theta)\ddot{\theta}=0 \tag{34}$$

where A_0, A_1 and A_2 can be written as:

$$A_0=(1-\mu\tan\beta)\left[k\left(\theta\text{-}\theta_0^*\right)-m_BgL_2\sin\theta-\right.$$
$$\left.F_BL_2\sin\theta\right]+\mu m_CgL_2\cos\theta+\mu m_CgL_2\sin\theta\tan\beta \tag{35}$$

$$A_1=-m_C L_2^2 \cos\theta \sin\theta - m_C \frac{L_2^3}{L_3} \cos\theta \sin^2\theta \sec\beta + m_C L_2^2 \cos^2\theta \tan\beta - m_C \frac{L_2^3}{L_3} \cos\theta \sin^2\theta \tan^2\beta \sec\beta - m_C L_2^2 \sin^2\theta \tan\beta - m_C \frac{L_2^3}{L_3} \sin^3\theta \tan\beta \sec\beta + m_C L_2^2 \sin\theta \cos\theta \tan^2\beta - m_C \frac{L_2^3}{L_3} \sin^3\theta \tan^3\beta \sec\beta \quad (36)$$

$$A_2=m_B L_2^2 - \mu m_B L_2^2 \tan\beta + m_C L_2^2 \cos^2\theta + 2m_C L_2^2 \cos\theta \sin\theta \tan\beta + m_C L_2^2 \sin^2\theta \tan^2\beta \quad (37)$$

Each term in A_0, A_1 and A_2 is divided by "$m_B L_2^2$" to prevent any instability at numerical solution process and the following constants in Eq. (38) are defined to obtain the new A_0, A_1 and A_2 as in Eqs. (39) – (41), respectively:

$$\lambda_1=\frac{L_2}{L_3};\ \lambda_2=\frac{L_4}{L_3};\ \lambda_3=\frac{m_C}{m_B};\ \lambda_4=\frac{k}{m_B L_2^2};\ \lambda_5=\frac{g}{L_2};\ \lambda_6=\frac{F_B}{m_B L_2} \quad (38)$$

$$A_0=(1-\mu\tan\beta)\left[\lambda_4(\theta-\theta_0^*) - (\lambda_5+\lambda_6)\sin\theta\right] + \mu\lambda_3\lambda_5 \frac{\cos(\theta-\beta)}{\cos\beta} \quad (39)$$

$$A_1=-\lambda_3 \frac{\cos(\theta-\beta)}{\cos^2\beta}\left[\sin(\theta-\beta) + \lambda_1 \frac{\sin^2\theta}{\cos^2\beta}\right] \quad (40)$$

$$A_2=1-\mu\tan\beta + \lambda_3\left(\frac{\cos^2(\theta-\beta)}{\cos^2\beta}\right) \quad (41)$$

3. SOLUTION OF NON-LINEAR DIFFERENTIAL EQUATION BY RUNGE-KUTTA METHOD

Eq. (34) is a second order non-linear differential equation. It can be solved by numerical methods where one of them is the 4th order Runge-Kutta Method [20]. In this method, the change in slopes of the first and second order differentials are evaluated at 4 different points for each individual discrete time interval: the beginning and end points as well as two intermediate points of an individual time interval. Initial conditions are defined by Eqs. (42) and (43).

$$\theta(t_0)=\theta_0 \quad (42)$$

$$\frac{d\theta}{dt}(t_0)=\omega(t_0)=\omega_0 \quad (43)$$

In the solution procedure, if the first order derivative of the crank angle θ is defined as in Eq. (44) then second order derivative of the crank angle θ can be defined by Eq. (45).

$$\frac{d\theta}{dt}=\omega=f_1(t,\theta,\omega) \quad (44)$$

$$\frac{d\omega}{dt}=\frac{d^2\theta}{dt^2}=f_2(t,\theta,\omega) \quad (45)$$

From Eq. (34), the second order derivative of the crank angle θ can easily be obtained as:

$$f_2=-\frac{A_1 f_1^2+A_0}{A_2} \quad (46)$$

The change in θ and ω in the discrete time interval "h" can be calculated by Eqs. (47) and (48), respectively.

$$\theta_{n+1}=\theta_n+\frac{1}{6}(\Delta\theta_1+2\Delta\theta_2+2\Delta\theta_3+\Delta\theta_4) \quad (47)$$

$$\omega_{n+1}=\omega_n+\frac{1}{6}(\Delta\omega_1+2\Delta\omega_2+2\Delta\omega_3+\Delta\omega_4) \quad (48)$$

In these equations, $\Delta\theta_1$ and $\Delta\omega_1$ represent the corresponding slope values multiplied by h at the beginning of the discrete time interval and calculated as in Eqs. (49) and (50), respectively.

$$\Delta\theta_1=hf_1(t_n,\theta_n,\omega_n) \quad (49)$$

$$\Delta\omega_1=hf_2(t_n,\theta_n,\omega_n) \quad (50)$$

$\Delta\theta_2$ and $\Delta\theta_3$ as well as $\Delta\omega_2$ and $\Delta\omega_3$ represent the corresponding slope values at the intermediate points of the discrete time interval ($t_n+h/2$) and calculated as in Eqs. (51)-(54), respectively.

$$\Delta\theta_2=hf_1\left(t_n+\frac{h}{2},\theta_n+\frac{\Delta\theta_1}{2},\omega_n+\frac{\Delta\omega_1}{2}\right) \quad (51)$$

$$\Delta\omega_2 = hf_2\left(t_n+\frac{h}{2},\theta_n+\frac{\Delta\theta_1}{2},\omega_n+\frac{\Delta\omega_1}{2}\right) \quad (52)$$

$$\Delta\theta_3 = hf_1\left(t_n+\frac{h}{2},\theta_n+\frac{\Delta\theta_2}{2},\omega_n+\frac{\Delta\omega_2}{2}\right) \quad (53)$$

$$\Delta\omega_3 = hf_2\left(t_n+\frac{h}{2},\theta_n+\frac{\Delta\theta_2}{2},\omega_n+\frac{\Delta\omega_2}{2}\right) \quad (54)$$

Lastly, $\Delta\theta_4$ and $\Delta\omega_4$ represent the corresponding slope values at the end of the discrete time interval and given as:

$$\Delta\theta_4 = hf_1(t_n+h,\theta_n+\Delta\theta_3,\omega_n+\Delta\omega_3) \quad (55)$$

$$\Delta\omega_4 = hf_2(t_n+h,\theta_n+\Delta\theta_3,\omega_n+\Delta\omega_3) \quad (56)$$

4. EXPERIMENTS

An experimental setup (Figure 3) is developed to validate the results obtained from numerical solution of the second order non-linear differential equation. The setup has a crank, a connecting rod and a piston sliding inside a channel. A spring is attached to the crank and the ground. On the crank and connecting rod pin, a bucket is assembled to add any external load. There is also a scale attached for representing the crank angular position instantaneously.

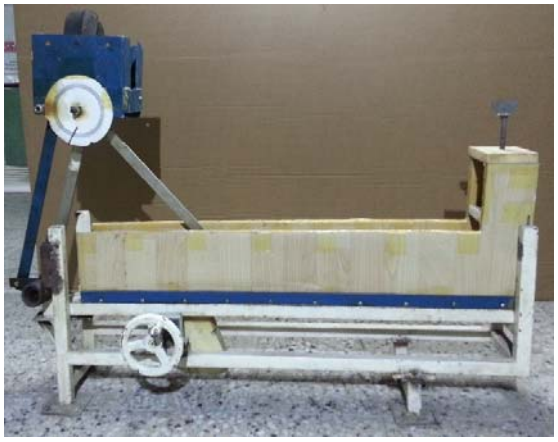

Figure 3. Experimental setup

Each experiment is recorded by a handy camcorder. The recorded videos are analyzed by a software program called "Movie Maker" such that each one second consists of 25 frames. Hence, the angular positon of the crank in each video frame is tracked for obtaining the piston position according to Eq. (25) at a particular time frame.

The physical as well as operational parameters of the experimental setup are tabulated in Table 1. Experiments are performed for 10 kg, 12 kg and 14 kg external loads as the only driving force added to the bucket. However, the bare mass of the bucket is 1,04 kg which should be added to the external load values. Experiments are carried for 3 different crank starting angular positions for each net external load applied (represented by M_B). The configuration of the experiments is also listed in Table 2 for ready reference.

Table 1. Physical and operational parameters for experiments

m_2 (kg)	0,96	L_2 (m)	0,45	k (Nm/r)	80
m_3 (kg)	0,96	L_3 (m)	0,45	μ	0,3
m_4 (kg)	0,76	L_4 (m)	0	F_B (N)	0
m_b (kg)	1,04	r_{G2} (m)	0,225	θ_0^* (°)	20
		r_{G3} (m)	0,225	ω_0 (r/s)	0

Table 2. Experiment configurations

	M_B = 11,04 kg	M_B = 13,04 kg	M_B = 15,04 kg
Exp. 1	$\theta = 20°$	$\theta = 20°$	$\theta = 20°$
Exp. 2	$\theta = 30°$	$\theta = 30°$	$\theta = 30°$
Exp. 3	$\theta = 40°$	$\theta = 40°$	$\theta = 40°$

5. RESULTS AND DISCUSSION

Results of experiments are obtained by analyzing each video frame as explained in previous section and tabulated in an Excel worksheet. Theoretical solutions for Eq. (34) are developed by applying the 4th order Runge-Kutta method as explained in Section 3. Hence, theoretical and experimental results are graphically shown in Figures 4-6. In Figure 4, theoretical and experimental results are

shown when 11,04 kg external load applied for three different crank starting angular positions values. Similarly, Figure 5 and Figure 6 present theoretical and experimental results graphically for external loads of 13,04 kg and 15,04 kg, respectively. In these figures, the effect of crank position at the start of motion for each externally added mass value can be explained as lower crank angles (steeper crank positions) yielding larger piston displacements in a longer duration. Also, the effect of externally added mass value can be observed as higher mass values producing larger piston displacement in a shorter duration.

The figures show that when crank starting angle is 30°, theoretical and experimental results very closely match for any three external load applied. Larger deviations are observed when crank starting angle is 20°.

At this point, it would be better to show the error percentage of experimental results against theoretical results. The error percentage for each experiment is calculated by the following equation:

$$\text{Error } \% = \frac{\text{Theoretical result} - \text{Experimental result}}{\text{Theoretical result}} * 100 \quad (57)$$

Figure 7 represents graphically the error percentage of each experimental result against the corresponding theoretical result. From this figure, error percentage of θ = 20° experiment for each external load depicts a considerable error level even though the error level keeps less than 10% until 0,4 seconds. Interestingly, error percentage of θ = 30° experiment for any external load is always less than 5% except only for higher loads. Finally, error percentage of θ = 40° experiments tend to yield higher errors at lower external load whereas higher external load results indicate to almost zero error. Therefore, the obtained results demonstrate that the proposed method can be regarded as reliable to analyze the dynamic effects of any slider-crank mechanism for securing a desired piston speed at particular piston positions. As an example, piston speed vs. piston position graphs for three different external loads are drawn for crank starting angle θ=30° in Figure 8 and similar graphs are drawn for three different crank starting angle values when M_B is kept constant at 13,04 kg, (Figure 9).

Analysis of Figure 8 clearly shows that an increase in the external load results in higher speeds in a wider range of piston displacement whereas in Figure 9 a decrease in the crank starting angle would result in higher piston speeds in a wider piston displacement.

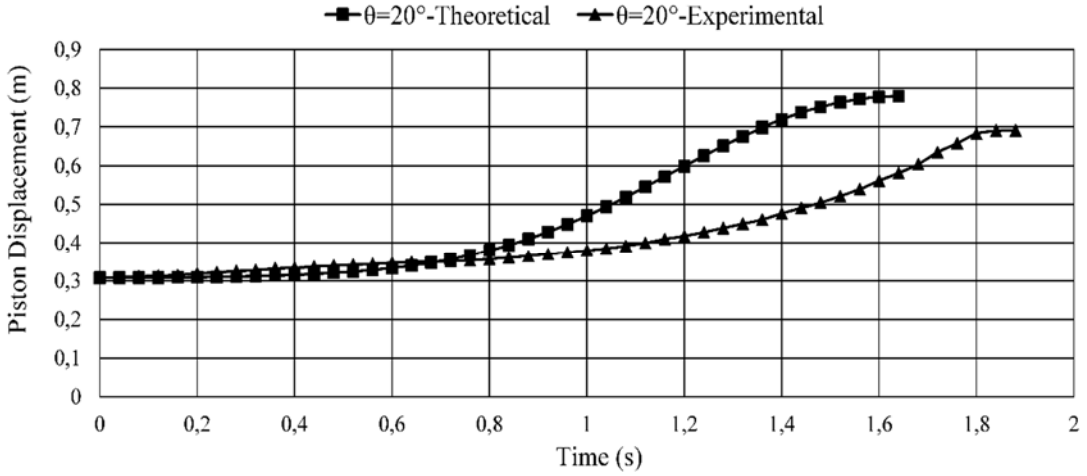

(a) Piston Displacement - Time graph for Mb=11,04kg and θ=20°

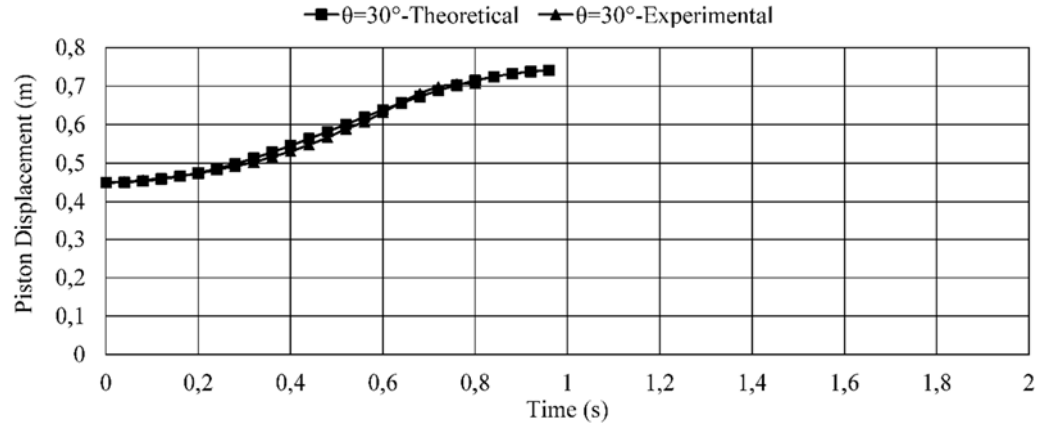

(b) Piston Displacement - Time graph for Mb=11,04kg and θ=30°

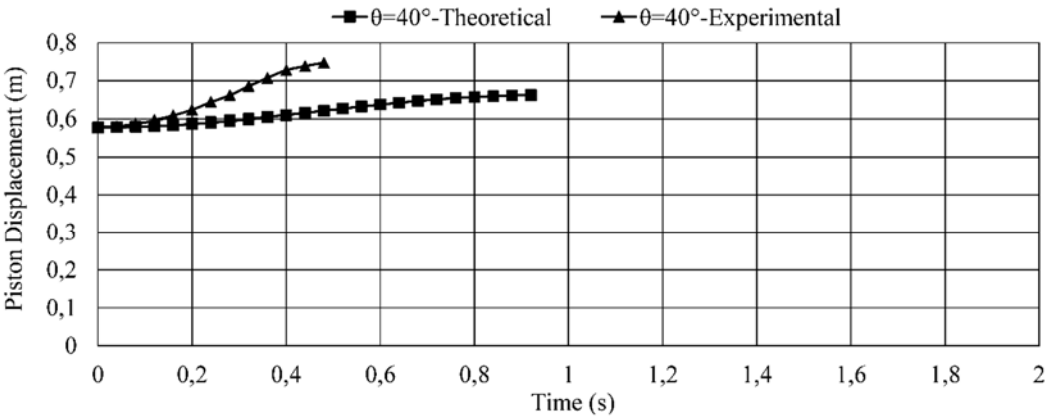

(c) Piston Displacement - Time graph for Mb=11,04kg and θ=40°

Figure 4. Comparison of theoretical and experimental results for 11,04 kg external load

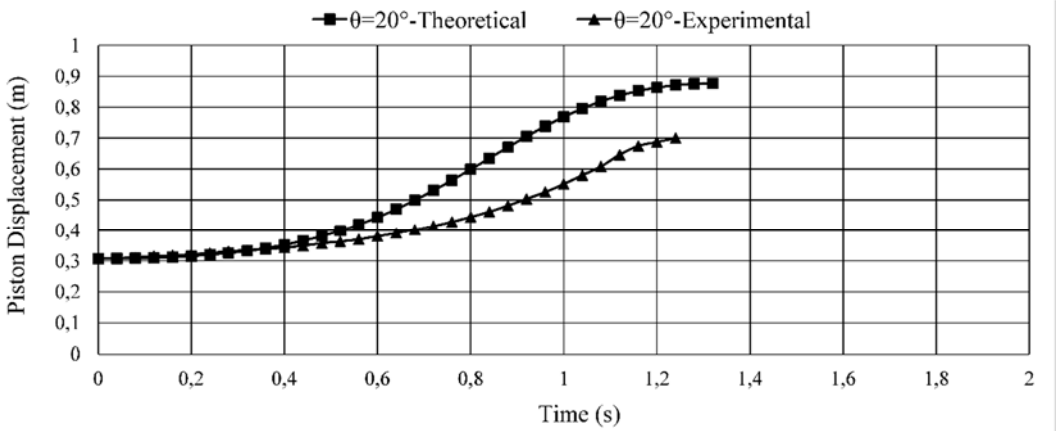

(a) Piston Displacement - Time graph for Mb=13,04kg and θ=20°

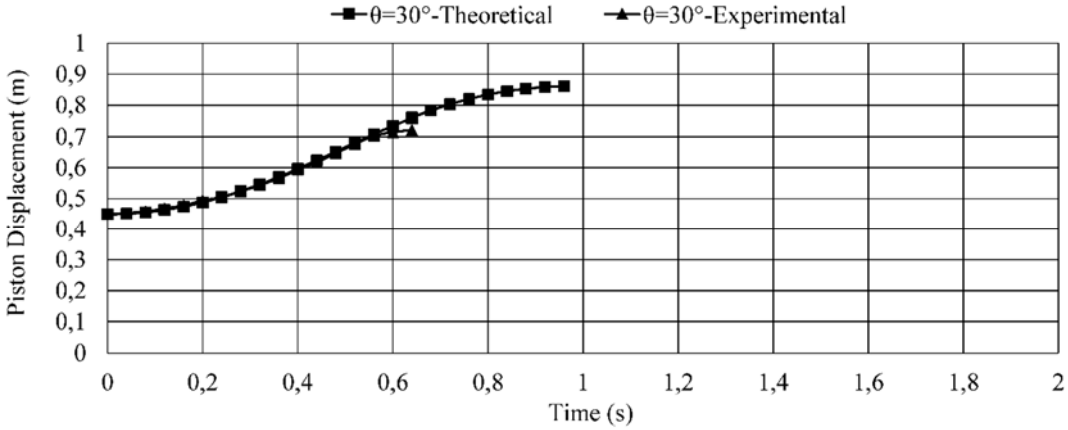

(b) Piston Displacement - Time graph for Mb=13,04kg and θ=30°

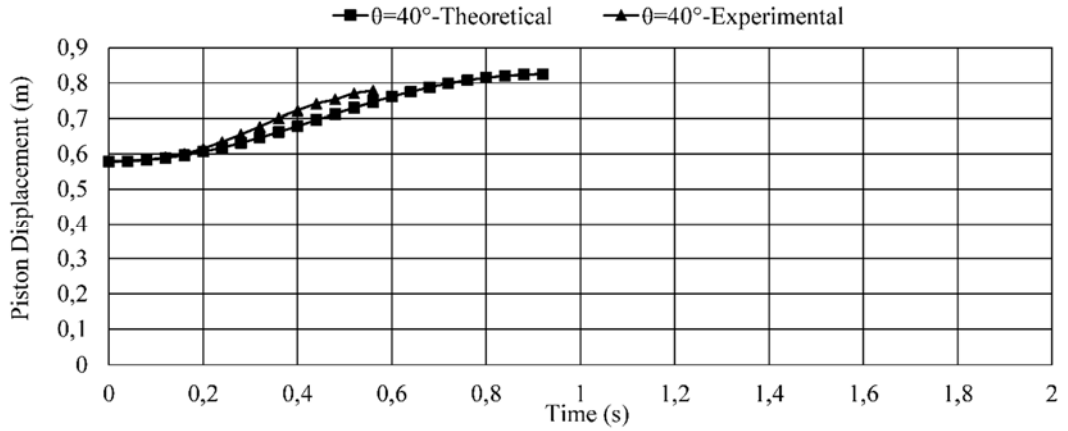

(c) Piston Displacement - Time graph for Mb=13,04kg and θ=40°

Figure 5. Comparison of theoretical and experimental results for 13,04 kg external load

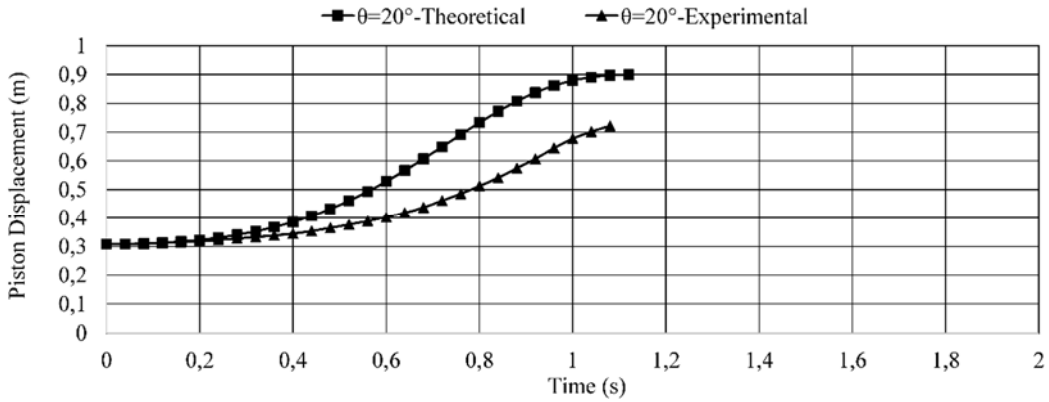

(a) Piston Displacement - Time graph for Mb=15,04kg and θ=20°

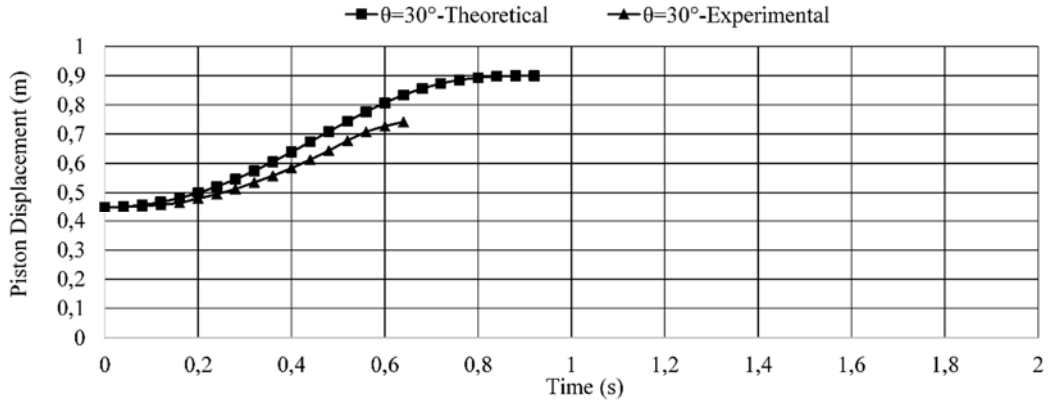

(b) Piston Displacement - Time graph for Mb=15,04kg and θ=30°

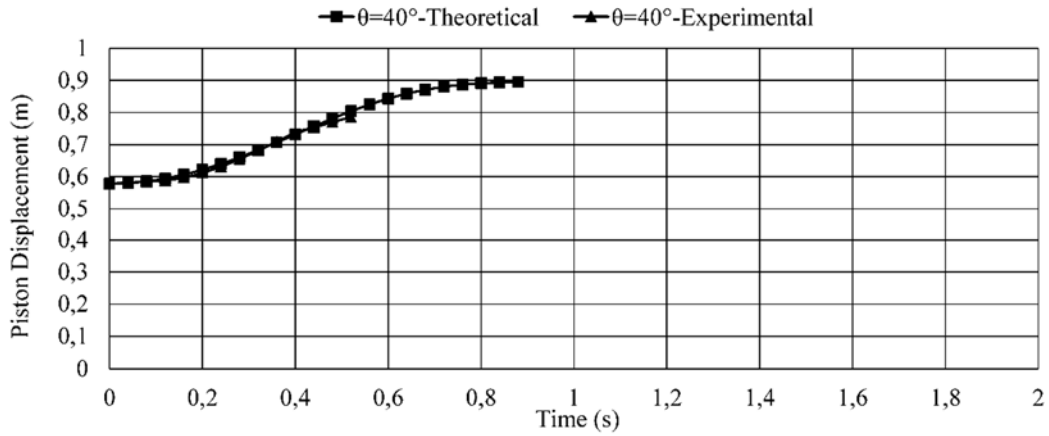

(c) Piston Displacement - Time graph for Mb=15,04kg and θ=40°

Figure 6. Comparison of theoretical and experimental results for 15,04 kg external load

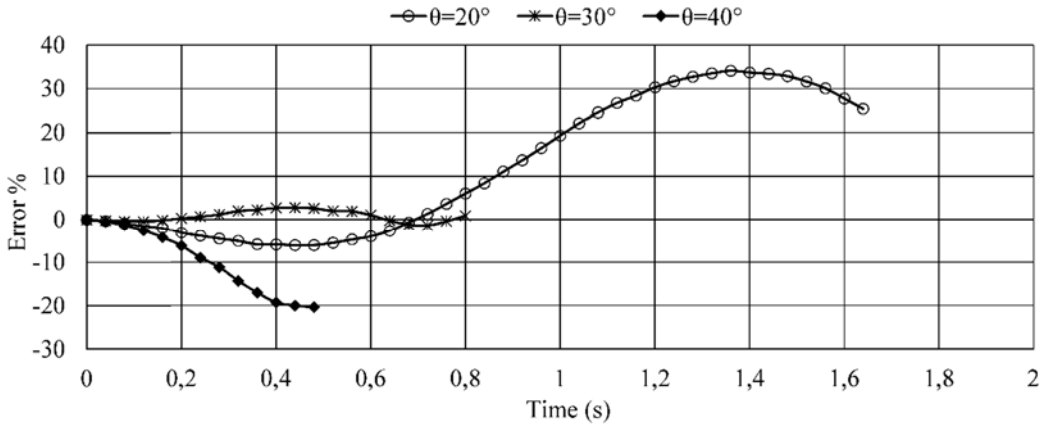

(a) Error %- Time graph for Mb=11,04kg and θ=20°, θ=30° and θ=40°

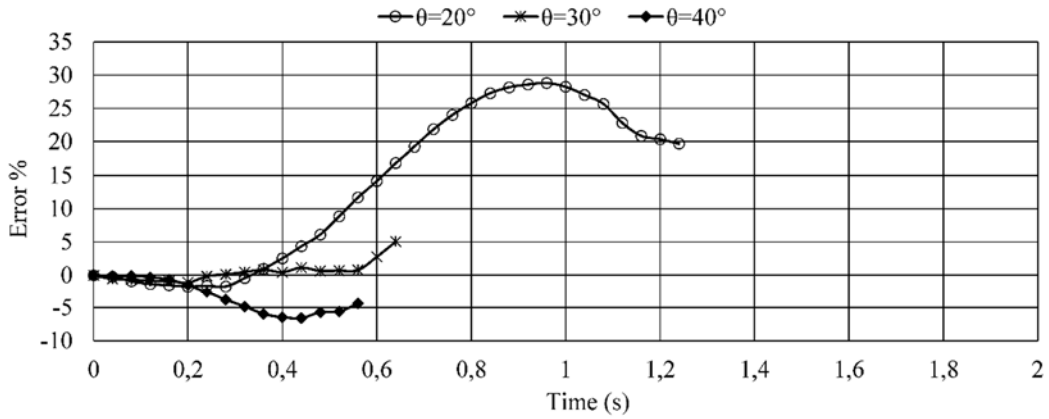

(b) Error %- Time graph for Mb=13,04kg and θ=20°, θ=30° and θ=40°

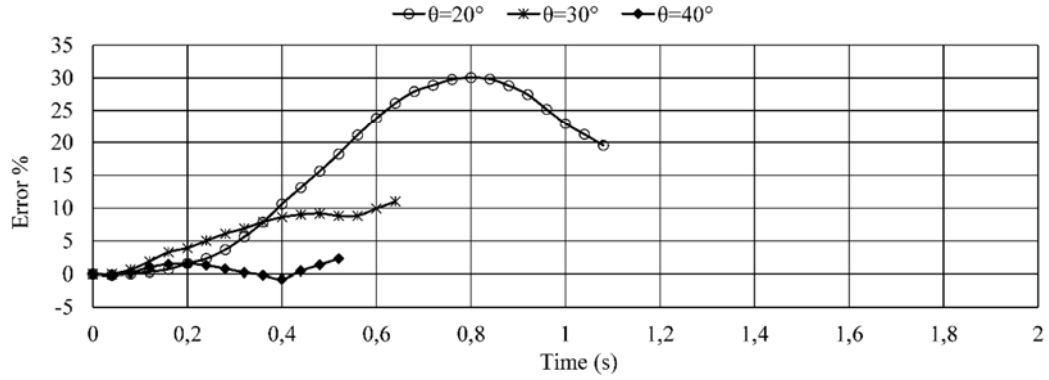

(c) Error %- Time graph for Mb=15,04kg and θ=20°, θ=30° and θ=40°

Figure 7. Comparison of error percentage of theoretical results against experimental results

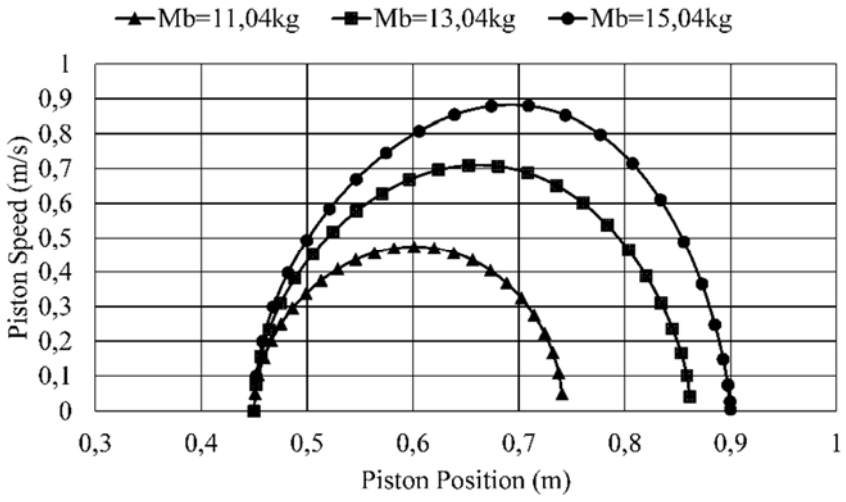

Figure 8. Analysis of External load M_B on piston speed vs. displacement for θ=30°

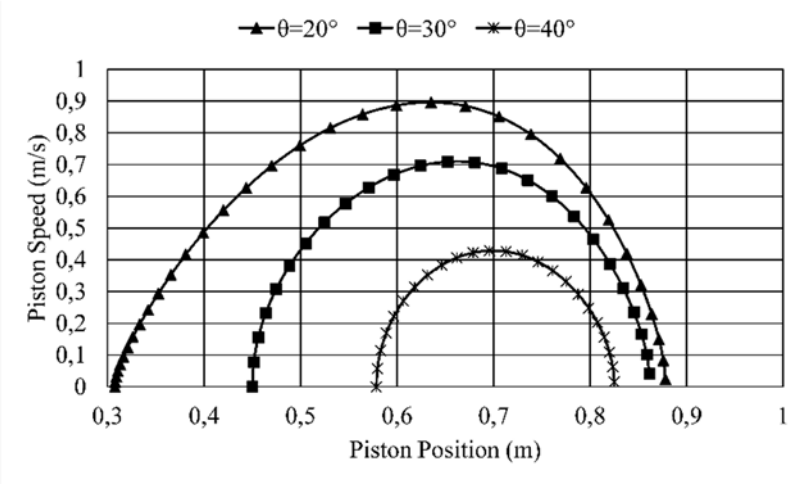

Figure 9. Analysis of crank starting angle θ on piston speed vs. displacement for M_B =13,04 kg

The problem at this point would be to choose appropriate piston positions where piston speed deviation constrained to a predetermined error level with respect to desired average speed. As an example, in Figure 8 or Figure 9, by considering the graph for M_B =13,04 kg and θ=30° as well as an acceptable maximum 5% deviation from average speed would yield a minimum speed of 0,64 m/s where the maximum speed is 0,71 m/s as well as a resultant average speed is 0,675 m/s. Hence, in the corresponding figures, the piston operation range would be identified as from 0,58 m to 0,74 m for the minimum speed. In this piston position range, the piston speed is restrained to 5% error.

Hence, the piston position vs. piston speed graphs can be evaluated by changing the dimensional and operational parameters until the acceptable piston speed in the required piston range is obtained.

6. CONCLUSION

Here in this work, against the force acting on the crank-pin of a slider-crank mechanism the dynamic behavior of the mechanism is modeled by lumped-mass approach to achieve the speed control of the piston. An experimental model under similar conditions was set up and experiments were carried out for comparative purposes. The difference between theoretical and experimental models were reasonably low to demonstrate the reliability of theoretical model. Nevertheless, the differences between the theoretical and experimental models can be explained by the following factors:

- The frictional effects at revolute joints.
- Three-dimensional effects of the moving gravitational loads added in the bucket on the accelerating slider towards the end of the fast experiments.
- Non-uniform and variable coefficient of friction between piston and ground.
- Lumped mass system not satisfying dynamic equivalence condition.
- The resolution and frame per second of the camera being not high enough.

If these factors are taken into account in continuous model of the dynamic behavior of the mechanism, then the opportunities of the speed control developed from the improved theoretical model will give a better opportunity to that end, which is a subject of future work.

7. REFERENCES

1. Vinogradov, O., 2000. Fundamentals of Kinematics and Dynamics of Machines and Mechanisms (1st ed.), CRC Press, Boca Raton (FL).

2. Myszka, D., 2012. Machines and Mechanisms, Applied Kinematic Analysis (4th ed.), Prentice Hall, Upper Saddle River (NJ).

3. Erdil, A.H., 1998. Buz Kalıplarından Kar Üretilmesi İçin Bir Makina Tasarımı, Yüksek Lisans Tezi, Çukurova Üniversitesi, Adana, 94.

4. Sarigecili, M.I., Akcali, I.D., 2018. Development of Constant Output–input Force Ratio in Slider–crank Mechanisms, Inverse Problems in Science and Engineering. (In Press) DOI: 10.1080/17415977.2018.1470625.

5. Franco, W., Iarussi, F., Quaglia, G., 2016. Human powered press for producing straw bales for use in construction during post-emergency conditions, Biosystems Engineering, 150, 170-181. DOI: 10.1016/j.biosystemseng.2016.08.007.

6. Halicioglu, R., Dulger, L.C., Bozdana, A.T., 2016. Structural Design and Analysis of a Servo Crank Press, Engineering Science and Technology, an International Journal, 19(4), 2060-2072. DOI: 10.1016/j.jestch.2016.08.008.

7. Erkaya, S., Su, Ş., Uzmay, İ., 2007. Dynamic Analysis of a Slider–crank Mechanism with Eccentric Connector and Planetary Gears, Mechanism and Machine Theory, 42(4), 393-408. DOI: 10.1016/j.mechmachtheory.2006.04.011.

8. Ha, J.L., Fung, R.F., Chen, K.Y., Hsien, S.C., 2006. Dynamic Modeling and Identification of a Slider-crank Mechanism, Journal of Sound and Vibration, 289(4–5), 1019-1044. DOI: 10.1016/j.jsv.2005.03.011.

9. Huang, M.S., Chen, K.Y., Fung, R.F., 2010. Comparison Between Mathematical Modeling and Experimental Identification of a Spatial Slider–crank Mechanism, Applied Mathematical Modelling, 34(8), 2059-2073. DOI: 10.1016/j.apm.2009.10.018.

10. Fung, R.F., Chiang, C.L., Chen, S.J., 2009. Dynamic Modelling of an Intermittent Slider–crank Mechanism, Applied Mathematical Modelling, 33, 2411-2420. DOI: 10.1016/j.apm.2008.07.004

11. Silva R., de C., Nunes, M.A.A., Bento, J.P.M., da Costa, V.E., 2013. Modelling an Inverted Slider Crank Mechanism Considering Kinematic Analysis and Multibody Aspects, Proceedings of the XV International Symposium on Dynamic Problems of Mechanics (DINAME 2013), Buzios, RJ, Brazil, 1-10.

12. Yan, H.S., Chen, W.R., 2000. On the Output Motion Characteristics of Variable Input Speed Servo-controlled Slider-crank Mechanisms, Mechanism and Machine Theory, 35(4), 541-561. DOI: 10.1016/S0094-114X(99)00023-3

13. Lin, F.J., Fung, R.F., Lin, H.H., Hong, C.M., 2001. A Supervisory Fuzzy Neural Network Controller for Slider-crank Mechanism, Mechatronics, 11(2), 227-250. DOI: 10.1016/S0957-4158(99)00070-7

14. Wai, R.J., Lin, F.J., 1998. A Fuzzy Neural Network Controller with Adaptive Learning Rates for Nonlinear Slider-crank Mechanism, Neurocomputing, 20(1–3), 295-320. DOI: 10.1016/S0925-2312(98)00022-8

15. Zhao, B., Dai, X.D., Zhang, Z.N., Xie, Y.B., 2016. A New Numerical Method for Piston Dynamics and Lubrication Analysis, Tribology International, 94, 395-408. DOI: 10.1016/j.triboint.2015.09.037

16. Reis, V.L., Daniel, G.B., Cavalca, K.L., 2014. Dynamic Analysis of a Lubricated Planar Slider–crank Mechanism Considering Friction and Hertz Contact Effects, Mechanism and Machine Theory, 74, 257-273. DOI: 10.1016/j.mechmachtheory.2013.11.009

17. Wang, Y.M., Chen, C.H., 2012. The Dynamics of a Slider-crank Mechanism with a Fourier-Series Based Axially Periodic Array Non-Homogeneous Coupler, Journal of Sound and Vibration, 331(22), 4831-4847. DOI: 10.1016/j.jsv.2012.05.025.

18. Akbari, S., Fallahi, F., Pirbodaghi, T., 2016. Dynamic Analysis and Controller Design for a Slider–crank Mechanism with Piezoelectric Actuators, Journal of Computational Design and Engineering, 3(4), 312-321. DOI: 10.1016/j.jcde.2016.05.002.

19. Hirschhorn, J., 1962. Kinematics and Dynamics of Plane Mechanisms (First ed.), McGraw-Hill New York.

20. Chapra, S.C., Canale, R.P., 2010. Numerical Methods for Engineers (Sixth ed.) McGraw-Hill, New York.